Near Threshold Photochemistry of Propanal. Barrier Height, Transition State Structure, and Product State Distributions for the HCO Channel

Gregory F. Metha,[†] Andrew C. Terentis,[‡] and Scott H. Kable*

School of Chemistry, University of Sydney, NSW, 2006, Australia

Received: February 1, 2002; In Final Form: April 16, 2002

The photodissociation dynamics of propanal have been investigated at photolysis wavelengths between 300 and 327 nm. The threshold for production of HCO fragments was found to be 326.26 nm, which corresponds to 30645 cm^{-1} (366.6 kJ mol^{-1}) above the zero-point of the S_0 state. From known thermochemical data, this threshold lies 25.0 ± 3.6 kJ mol^{-1} above the bond dissociation energy. The nascent HCO rotational and translational energy distributions were determined following dissociation at threshold. The rotational population was measured as a function of N, K_a, K_c, and S. The distribution of rotational states followed a Gaussian function with an average rotational energy of 2.5 ± 0.5 kJ mol^{-1}. The population of the near-degenerate spin-rotation states was equal, while the population in the asymmetry doublets favored the upper energy component by about 3:1. Careful measurement of the Doppler profiles of individual $K_a = 0$ lines in the LIF spectrum revealed that the translational energy also shows a Gaussian-like distribution with an average energy of 6.5 ± 1.0 kJ mol^{-1}. The ethyl fragment must also have an average translational energy of 6.5 ± 1.0 kJ mol^{-1} and therefore an average internal energy of 9.5 kJ mol^{-1} is inferred. The observed energy partitioning in the fragments is consistent with a model in which the HCO rotational and translational excitation is determined mostly by the transition state geometry, a barrier on the triplet surface, and the fixed energy in the exit channel. A modified impulsive model was satisfactory in reproducing the energy deposited into the various degrees of freedom. The model implied impact parameters at infinite separation corresponding to an in-plane HCO angle of 40° and an out-of-plane angle of 60°. The strongly pyramidal nature of the transition state produces more angular momentum about the *b* axis than the *c* axis, which causes the preference for the upper energy component of the asymmetry doublets.

Introduction

The UV photochemistry of aliphatic aldehydes has been extensively researched over the past few decades.[1−5] Much of this interest has been fueled by the presence of these molecules in the atmosphere.[6,7] The aldehydes enter the atmosphere either directly as constituents of vehicle exhaust or, more ubiquitously, as oxidation products of other organic pollutants such as saturated hydrocarbons. Their UV photochemistry is characterized by two major chemical pathways, one producing radical species and the other producing molecular species:

$$RCHO + h\nu \rightarrow R + HCO \text{ (radical channel)} \quad (1)$$

$$\rightarrow RH + CO \text{ (molecular channel)} \quad (2)$$

where R = H, CH_3, and CH_3CH_2 in the case of formaldehyde, acetaldehyde, and propanal, respectively. The radical channel is particularly important in the initiation of radical chain reactions that lead to photochemical smog formation in the polluted urban troposphere.[6]

These two photodissociation channels have been investigated thoroughly and are now quite well understood.[1,7−11] Both reactions occur via a weak $S_1 \leftarrow S_0$ (n, π^*) transition appearing in the spectral region 240−360 nm. Upon excitation, the molecular structure is altered, resulting in an increased CO bond length and a breakdown of the planarity of the HCO moiety relative to the remainder of the molecule.[12,13]

After photoexcitation into the S_1 state,

$$S_0 + h\nu \rightarrow S_1^* \quad (3)$$

several photophysical processes are possible which can be summarized as follows:[4,14]

$$S_1^* \rightarrow S_0 + h\nu' \quad (4)$$

$$\rightarrow S_0^* \text{ (IC)} \quad (5)$$

$$\rightarrow T_1^* \text{ (ISC)} \quad (6)$$

Apart from fluorescing back into the ground state, the nonradiative processes of internal conversion (IC) and intersystem crossing (ISC) are induced by vibronic and spin−orbit coupling between S_1 and the lower-lying S_0 and T_1 states. Since the efficiency of these latter processes is dependent on the density of states, they have been found to be more dominant in the larger aldehydes. In the case of fomaldehyde, the density of states is sufficiently small that coupling is relatively weak, leading to completely different photochemical behavior compared with acetaldehyde, propanal, and larger aldehydes.[15] For acetaldehyde and propanal, the total rate of nonradiative processes (IC + ISC) is about 3 orders of magnitude larger than the radiative rate.[1,5] Furthermore, it is now established that

* Author to whom correspondence should be addressed. E-mail: S.Kable@chem.usyd.edu.au.

[†] Current address: Department of Chemistry, University of Adelaide, Adelaide, South Australia, 5005, Australia.

[‡] Current address: Department of Chemistry, The University of Arizona, Tucson, AZ 85721.

10.1021/jp025590x CCC: $22.00
Published on Web 05/25/2002

for these molecules, IC into S_0* leads to dissociation via reaction 2 to produce molecular products and that ISC into T_1* leads to radical formation via reaction 1.[5,16]

The photochemistry of acetaldehyde has been studied over several decades.[17−24] At 308 nm, radical production via reaction 1 is by far the most important process, with a quantum yield of 0.90−0.95. Hanazaki and co-workers have performed several studies of the photodissociation of jet-cooled acetaldehyde[20−22] to show that the fluorescence quantum yield drops markedly for $\lambda < 317.3$ nm ($E > 377.3$ kJ mol^{-1}). Furthermore, the photofragment excitation spectrum demonstrated a discreet threshold for HCO production at 320.5 nm (373.4 kJ mol^{-1}), which was interpreted as corresponding to the height of the barrier on the T_1 surface.

Rotational distributions of nascent HCO have been reported at various wavelengths[22,24] and found to follow Boltzmann-like behavior with an estimated average rotational energy of ∼7 kJ mol^{-1} at all wavelengths. Average translational distributions extracted from an analysis of Doppler widths at 308 nm were found to be ∼11 kJ mol^{-1} and a translational energy of 21 kJ mol^{-1} was inferred for the methyl fragment. Subsequent work by Lee and Chen,[23] at several excitation wavelengths, found that the rotational distributions of HCO follow a Gaussian distribution with the energy partitioned differently along the *a*, *b*, and *c* axes. A very detailed analysis of the product rotational state distribution revealed that, for $K_a = 1$, there is a preferential population within the asymmetry doublets for the higher energy component, N_1^u (which has $K_c = N - 1$), relative to the lower energy component, N_1^l (with $K_c = N$), with a maximum ratio of populations of 3.7 at $N = 12$. (As a radical, HCO has an unpaired electron with spin $S = 1/2$. The angular momentum of the nuclear framework is given the symbol, N, while J is used for the total angular momentum, i.e. $J = N + S$.) This K_c dependence, along with the observed rotational distributions, indicated that the HCO fragment was recoiling with angular momentum preferentially aligned along the *b* rather than *c* axis from a transition state with the HCO moiety bent about 60° out-of-plane.

In comparison with acetaldehyde, the spectroscopy, photochemistry, and particularly reaction dynamics of propanal remains less explored. The addition of a methylene group introduces the complexity that several rotational conformers are now possible. Spectroscopic and theoretical work have shown that two stable conformers exist in the ground electronic state.[13,25−32] In the cis conformation, the methyl group is eclipsed with the oxygen atom (OCCC dihedral angle = 0°) whereas the skew conformation has the OCCC dihedral angle at approximately 128°. The cis conformer is found to be more stable by 5 kJ mol^{-1} with a barrier of 9 kJ mol^{-1} separating the cis and skew minima.[31] The structure of propanal in the S_1 state has been investigated theoretically and spectroscopically.[12,33−35] The origin of the $S_1 \leftarrow S_0$ (n, π^*) transition was first proposed to be 29 258 cm^{-1} from UV absorption studies,[12] subsequently revised to 30 064 cm^{-1} following LIF studies in a supersonic expansion,[34] which supports a rich vibronic structure. Very little is known about the other excited states of propanal and information about the T_1 state is scarce or nonexistent. Recently, there have been several experimental and theoretical investigations of the $S_2 \leftarrow S_0$ (n, 3s) Rydberg transition,[30,36,37] which is near 185 nm, and therefore plays no part in the photochemistry discussed herein.

The photochemical studies that have been carried out to date indicate that there are many similarities between acetaldehyde and propanal and maybe even longer-chain aliphatic aldehydes. The quantum yields (ϕ) for reactions 1 and 2 have been measured previously as a function of wavelength, pressure, and temperature with the former being dominant at low excitation energy.[38−40] At higher excitation energies, it was found that reaction 1 decreases and reaction 2 increases in importance. In the low-pressure limit, ϕ_1 was measured to be unity at 313 nm and at $\lambda = 254$ nm the quantum yields for reactions 1 and 2 were found to be 0.61 and 0.39, respectively. On the basis of excited-state quenching experiments, it was confirmed that the dominant nonradiative process from the S_1 state is ISC to T_1 resulting in radical formation via reaction 1. It was also confirmed that the molecular channel, reaction 2, occurs from upper vibrational levels S_0* following IC from S_1*.

More recently, we have investigated the photodissociation dynamics of propanal at 309.1 nm by monitoring the nascent HCO population distribution of N and K_a states via LIF spectroscopy.[41,42] The population distribution of N and K_a states could be reasonably characterized by a Boltzmann distribution with a temperature of 480 ± 50 K corresponding to an average rotational energy of 6.0 ± 0.6 kJ mol^{-1}. An examination of the Doppler profiles of a number of transitions led to the conclusion that the majority of excess energy was partitioned into HCO and ethyl translational motion, the average being 23 ± 4 kJ mol^{-1}, and that the ethyl fragment contains very little internal energy. This work also led to the estimate that the barrier to radical production lay 15 kJ mol^{-1} below the photon energy (i.e., 372 kJ mol^{-1} or 321.6 nm). No evidence for excited vibrational population was found.

This present work continues our study into the dynamics of the $CH_3CH_2CHO + h\nu \rightarrow CH_3CH_2 + HCO$ reaction channel in order to explore three key aspects. First, we establish the energy threshold to radical formation, which corresponds to the energy barrier for the cleavage of the C−C bond. Second, we interpret the dynamics of the reaction on the triplet surface using impulsive models. Finally, we examine the detailed populations within the K_c doublets in the same manner as for acetaldehyde[23] to explore whether this "K_c effect" remains an important component of the product state distributions even for a relatively large photochemical system.

Experimental Section

The experimental details are similar to those used in our previous study.[41] In brief, 2 atm of helium was passed over a reservoir of propanal immersed in an ice bath maintained at 0 °C. The ensuing ∼5% propanal vapor in helium mix was expanded through a 0.5 mm orifice of a pulsed nozzle (Precision Instruments, PV-M3) into a vacuum chamber. Two perpendicular unfocused laser beams crossed the free supersonic expansion approximately 8 mm from the nozzle orifice. The first laser was a Continuum (Surelight II-10) Nd:YAG laser pumping a Lambda Physik (Scanmate) dye laser. DCM dye and a KDP doubling crystal produced 3−5 mJ/pulse of tunable light around 326 nm used here to dissociate the propanal molecules. The second laser was an excimer pumped dye laser system (Lambda Physik Lextra 200 and PD 2001E dye laser). Coumarin 503 dye, an intracavity Etalon, and a BBO doubling crystal produced 100−200 μJ/pulse of light in the range 250−265 nm with a resolution of ≈0.05 cm^{-1} suitable to probe HCO fragments. The probe laser crossed the free jet some 100 ns after the photolysis pulse. The pulse-to-pulse stability of whichever laser system was being scanned was monitored by guiding the laser beam after exiting the chamber onto a dye cuvette containing R6G dye in ethylene glycol. The visible fluorescence from the dye was monitored by a fast photodiode.

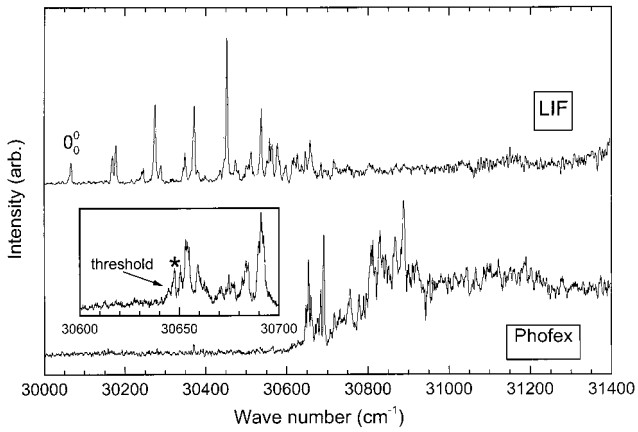

Figure 1. Laser-induced fluorescence and photofragment excitation spectra of propanal. The inset is an expanded view of the phofex spectrum near the threshold for observation of HCO fragments. The first peak in the inset spectrum is marked as "threshold". The position of propanal excitation for these experiments is indicated by an asterisk.

Propanal or formyl fluorescence was detected by an EMI 8938QB photomultiplier via a Spex Minimate monochromator set with broad slits and used as a tunable 20 nm band-pass filter to remove scattered laser light. The monochromator provides coarse vibrational resolution of the fluorescence but no rotational resolution. The signal was passed to a SRS-250 boxcar averager and gated integrator, averaged (typically 10 shots), and passed to a personal computer for data processing. The signal from the photodiode monitoring laser power was sent to a PAR 162/165 boxcar, thence to the same computer for shot-to-shot normalization of the signal. Timing of both lasers, the nozzle opening, and the detection electronics were controlled by a Stanford DG-535 digital delay generator. Timing and signal was continuously monitored on a Tektronix TDS-320 digital oscilloscope.

Results

(a) LIF and Photofragment Excitation Spectrum of Propanal. Figure 1 shows both a LIF and a photofragment excitation (phofex) spectrum of propanal, which was obtained by setting the probe laser to monitor the $^qR_0(3,4)$ bandhead of the origin band in the $\tilde{B} \leftarrow \tilde{X}$ transition of HCO (see below). The LIF spectrum shows several vibrational progressions built upon an origin at 30 064 cm^{-1} which have been assigned, in part, previously.[33,34] The spectrum is similar to the previous work and there is no evidence of absorption due to clusters in the expansion. The vibrational structure in the spectrum disappears for transitions to levels higher than 30 670 cm^{-1}. However, fluorescence emission does not cease. There is a weak, diffuse background that continues even beyond the region of the spectrum in Figure 1. The phofex spectrum shows no features below 30 640 cm^{-1}. From 30 645 to 30 700 cm^{-1} there are several intense, sharp bands, whose position agrees reasonably with some of the sharp bands in the LIF spectrum above. This sharp structure continues in the phofex spectrum until 30 900 cm^{-1} but with increasing energy it becomes broader and more congested.

We interpret these two excitation spectra as probing the same electronic state, viz. the S_1 or $\tilde{A}$ state of propanal. Above 30 645 cm^{-1} a new photophysical pathway opens up, which reduces the fluorescence quantum yield. The phofex spectrum shows that this pathway leads to production of HCO. The first identifiable peak in the phofex spectrum is located at 30 645 cm^{-1} and is marked by an arrow in Figure 1. We associate this peak with the threshold for the production of HCO. By analogy with acetaldehyde,[22,23] it probably corresponds to the top of the barrier to C−C bond cleavage on the T_1 surface.

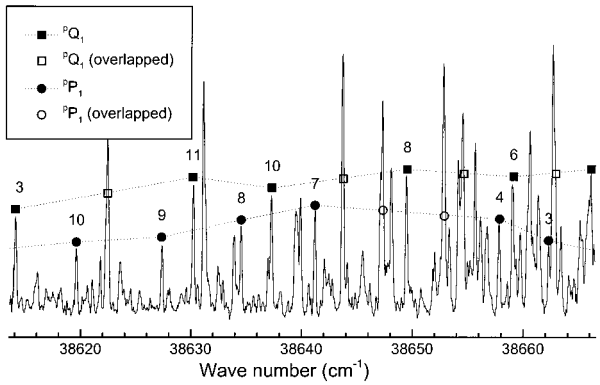

Figure 2. A portion of the nascent HCO LIF spectrum after dissociation of propanal. Two of the many rotational branches are assigned: the $^pQ_1$ and $^pP_1$. The $^pQ_1$ sub-branch probes exclusively N_1^u, while the $^pP_1$ sub-branch probes exclusively N_1^l.

(b) LIF Spectrum of Nascent HCO. The $\tilde{B} \leftarrow \tilde{X}$ electronic transition of HCO is a hybrid *a*/*b*-type transition of a near prolate rotor. The hybrid nature of the electronic transition means that all nine rotational branches resulting from the $\Delta K = 0, \pm 1$ and $\Delta N = 0, \pm 1$ selection rules are present, with the *a*-type transitions ($\Delta K = 0$ and $\Delta N = 0, \pm 1$) being the stronger. The asymmetry and spin-rotation splitting of the levels results in the *N* structure in many of the branches separating into doublets, triplets or quartets. In general, therefore, rotational populations can be probed as a function of the different spin-rotation and asymmetry quantum numbers.

The LIF spectrum of nascent HCO was measured after exciting propanal at 30 649 cm^{-1} which corresponds to the first moderately large peak in the phofex spectrum (marked with an asterisk in the inset to Figure 1). Transitions were observed arising from only the ground vibrational state of HCO, despite searching for the appearance of known hot-bands.[23,46−49] We concentrated our attention on the origin transition, $\tilde{B}(0,0,0) \leftarrow \tilde{X}(0,0,0)$, which has an appearance similar to HCO spectra that have been published previously following dissociation of propanal,[41] propenal,[50] acetaldehyde,[23,24] and formaldehyde.[42−45] The spectrum is complex because of the number of rotational branches and the multiple splittings caused by spin-rotation and similar asymmetry. Figure 2 shows a small region of the HCO spectrum to indicate the typical congestion prevalent throughout the entire spectrum. Only the $^pQ_1$ (indicated by squares) and $^pP_1$ (circles) sub-branches are assigned because they highlight the difference in K_c population, which is dealt with in some detail later. The filled symbols are transitions free from overlap and suitable for extracting rotational populations. The open symbols are transitions that suffer overlap from other branches and are not used to extract populations. Every peak in the HCO spectrum can be assigned with confidence, although many are overlapping. Our assignments exactly follow the previous papers and we will not dwell further upon the details of the assignment but refer the reader to Chen's papers on HCO spectroscopy.[23,46−49]

(c) Rotational State Distributions. The $\tilde{B}$ state of HCO is affected by at least two perturbations that affect the intensities of the transitions. The $\tilde{B}$ and $\tilde{X}$ states are coupled, which leads to a fluorescence quantum yield that generally gets smaller with *N* and K_a but is irregular. Within the $\tilde{B}(0,0,0)$ vibronic state, Chen et al. have measured the fluorescence lifetimes for almost every rotational level that we have accessed here, and we use

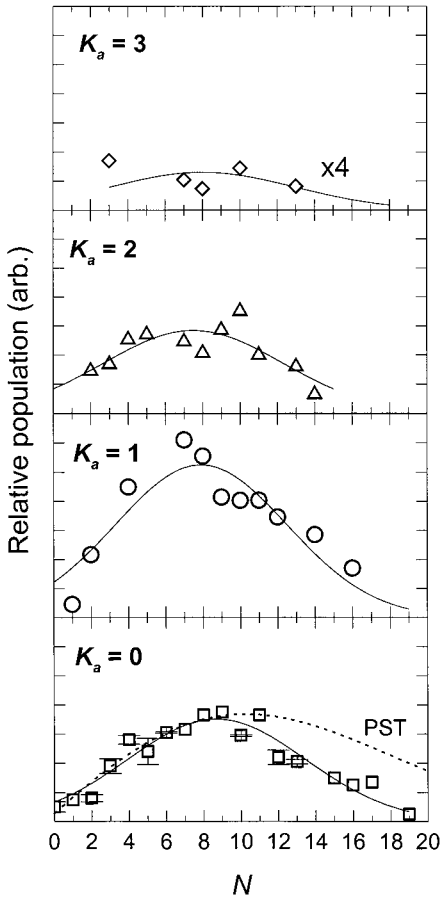

Figure 3. HCO product state distributions for $K_a = 0-3$ as a function of N following the excitation of propanal near threshold (30 649 cm^{-1}). The distributions are averaged over both J and K_c. Gaussian and PST fits to the distributions are shown as continuous and dashed lines, respectively.

their lifetimes to correct for this variation in quantum yield. In addition, the intensities are affected by Coriolis coupling and axis-switching.[23,46−51] The *a*-type Coriolis coupling between the $\tilde{B}$ and $\tilde{A}$ states of HCO leads to an increase in intensity of transitions that terminate in $K_a' = 1$ states over the $K_a' = 0$ states. Axis-switching (rotation of the inertial axes between the $\tilde{X}$ and $\tilde{B}$ states) causes intensities in the *P*, *Q*, and *R* transitions to vary from the Hönl-London formulas. Despite this, reliable rotational populations can be obtained providing the correct axis-switching line strengths are used,[23,51] the fluorescence quantum allowed for,[23] and the empirical corrections for different K_a states applied.[23]

The integrated peak intensities were recorded for all non-overlapping transitions. Where peaks were overlapping, the area of component peaks were obtained by deconvoluting the peaks assuming each to be a Gaussian peak profile with a width parameter of $\sigma = 0.17$ cm^{-1} (see section on translational energy below). To obtain relative population distributions these peak areas were divided by the linestrength factors, including the effect of axis-switching.[23] The values were then divided by the upper state fluorescence lifetimes, which are available as a function of N, K_a, K_c, J, also from the work of the Chen group. Finally, these values were divided by 0.81 for $K_a = 1$, 0.43 for $K_a = 2$, and 0.25 for $K_a = 3$ to allow for the Coriolis effect (the $K_a = 1$ and 2 values are from the work of Chen,[23] whereas $K_a = 3$ is estimated in the same manner as previously[24]).

Figure 3 shows the HCO rotational state population distributions as a function of N separated out for each K_a. The scale on the ordinate is the same for all four panels and the error bars for the $K_a = 0$ data represent the total range of population values extracted from various rotational branches. The N quantum number distributions range from 0 to 19 with a maximum around $N = 9$. Each distribution has been fitted to a Gaussian function, which is shown as a continuous line.

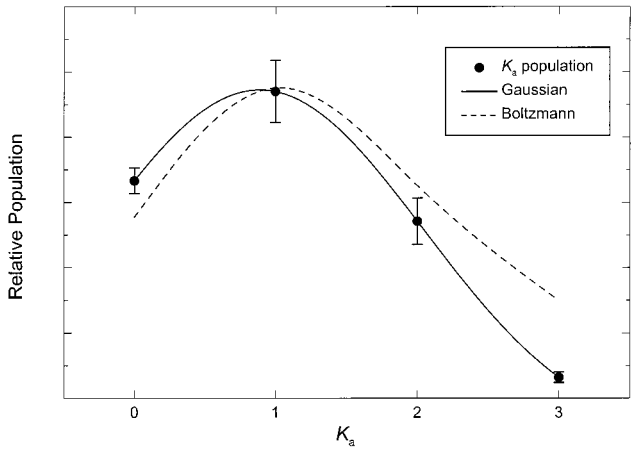

Figure 4. HCO product state distributions as a function of K_a following the excitation of propanal near threshold (30 649 cm^{-1}). Gaussian and Boltzmann fits to the distributions are shown as continuous and dashed lines, respectively.

A comparison of the rotational population distribution as a function of K_a shows that most population resides in the $K_a = 1$ manifold. The $K_a = 0$ and 2 manifolds are approximately equally populated but there is minimal population in states with $K_a = 3$ and no observed population in higher K_a states. This is shown more clearly in Figure 4 where the integrated population over N for each K_a is plotted. The resultant distribution is again fitted to a Gaussian function as a solid line.

From the rotational energy distribution, using the Gaussian fit where no specific N, K_a data are available, we can now calculate the *average* rotational energy for HCO, $\langle E_{rot} \rangle$, over all N and K_a, which is defined simply as:

$$\langle E_{rot} \rangle = \frac{\sum (\text{Population} \times E_{rot})}{\sum \text{Population}}$$

and results in an average rotational energy of 2.5 ± 0.5 kJ mol^{-1}.

Each rotational (N, K_a) state can be split into asymmetry (K_c) and spin-rotation (S) components, and the rotational distributions can be determined separately to examine these effects. With respect to spin-rotation, we have found the relative populations to be independent of $S = \pm 1/2$ for all cases where we can spectrally resolve the splitting. This is consistent with what has been previously observed in the photodissociation of formaldehyde,[45] acetaldehyde,[23] and propenal.[50] Once again we conclude that the electron spin of HCO is not influenced by the dynamics of the reaction. This is understandable given the small magnitude of the spin-rotation coupling, which therefore implies the electron spin angular momentum is essentially uncoupled to the angular momentum of the nuclear framework.

For each $K_a > 0$ level, there are two asymmetry components that are distinguished by the K_c quantum number. The HCO spectrum has several $K_a = 1$ transitions in which the asymmetry doublets are sufficiently resolved to determine separate population distributions. Figure 5 shows the population distribution within the asymmetry doublets for $K_a = 1$. The upper energy doublet state is labeled, N_1^u and the lower energy state, N_1^l. States in the N_1^u set always have $K_c = N - 1$ while the N_1^l

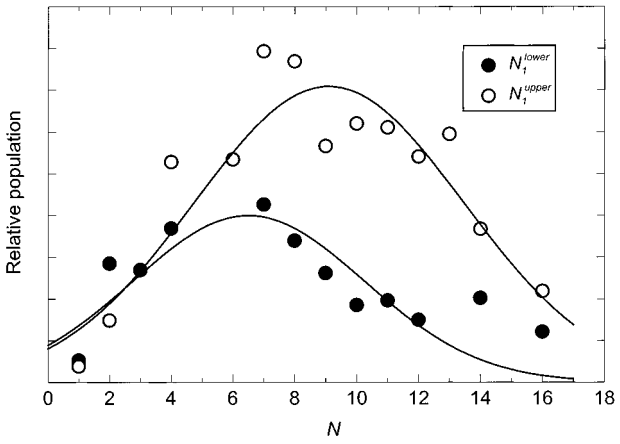

Figure 5. HCO product state distributions for $K_a = 1$ as a function of N following the excitation of propanal at threshold (30 649 cm^{-1}). The distributions are distinguished as arising from either N_1^u [●] or N_1^l [○]. A Gaussian fit to each distribution is shown as a continuous line.

states have $K_c = N$. The data in Figure 5 show an enhanced population for N_1^u levels, where in some instances, as much as a 3-fold preference is observed. This enhancement of N_1^u over N_1^l is exactly the same sense as that observed in acetaldehyde[23] and will be discussed later.

The asymmetry splitting decreases as a function of increasing K_a. In our experiment, with Doppler widths of ~0.17 cm^{-1}, the asymmetry splitting is unresolved in the $K_a = 2$ branches for $N < 10$. The few transitions we observe with $N > 10$ are too weak and/or overlapped for meaningful populations to be derived. Transitions arising from $K_a > 2$ are never K_c-resolved in our spectrum. Therefore, all subsequent discussion on these populations will be averaged over the K_c asymmetry pairs.

(d) Translational Energy. An estimate for the translational energy distribution of the recoiling HCO fragments can be achieved from a careful examination of the Doppler broadening in a single rotational transition (i.e., having complete spin-rotation and asymmetry resolution). An experimental profile is shown in Figure 6a) for the $^qR_0$ (13) transition and is typical of several transitions we have measured throughout the spectrum. The profile can be thought of as a convolution of: (i) the Doppler shift due to the recoil velocity of the HCO fragment, (ii) the Doppler width due to the transverse velocity distribution of the parent molecules, and (iii) the laser line width. The laser line width, σ, in our apparatus is known quite well from rotationally resolved LIF spectra of jet-cooled formaldehyde and the pump−probe laser geometry was chosen to minimize the effect of parent transverse velocity. Our best estimate of the instrument function for the probe laser is a Gaussian profile with $\sigma = 0.08-0.10$ cm^{-1} (σ is related to the full width at half-maximum by a factor $\sqrt{2\ln 2}$).

To recover the HCO translational energy distribution, we have deconvolved the laser function from the experimental profile. This process involves Fourier transform methods and can be achieved only on experimental data of high quality. The raw data (dots in Figure 6) are the average of many experimental traces, yet are still sufficiently noisy to make direct deconvolution impractical. The profile is quite well defined, even by eye, and so deconvolution of a smoothed experimental profile seems reasonable. The smoothing technique, however, needs to be chosen carefully; a moving average tends to broaden the peak, while a Fourier smooth is not so appropriate because some of the high frequency components at the shoulder of the peak are important to retain. The experimental profile obviously

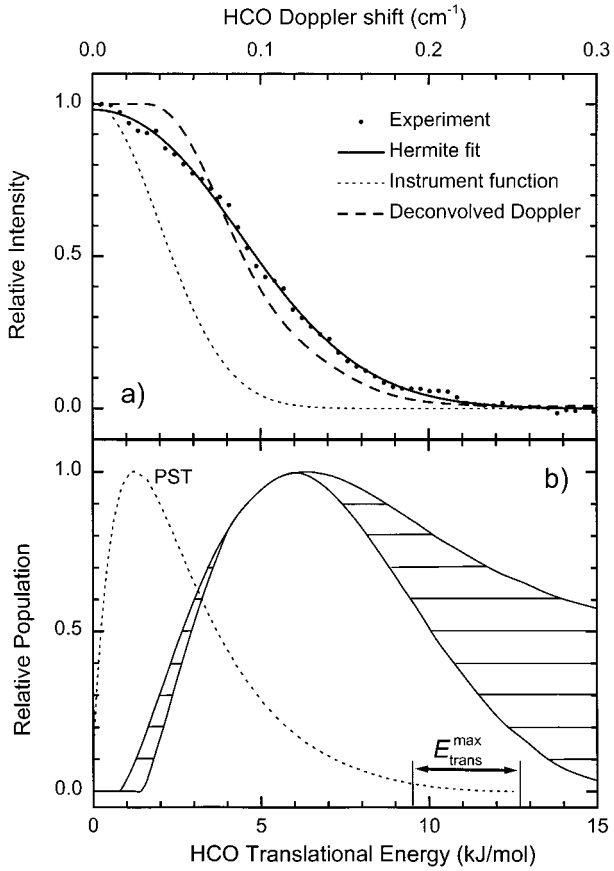

Figure 6. (a) Doppler profile of the $^qR_0(13)$ transition in the nascent HCO spectrum. A fit to the data using the two lowest even Hermite functions is shown as a solid curve and an instrument function by a dotted curve. The dashed curve is the deconvolution of the fitted function from the instrument function. (b) HCO translational energy distribution from the deconvolved data using a range of instrument functions. A PST calculation is shown as a dotted line for comparison.

resembles a Gaussian function and so a series of even Hermite polynomials (H_0, H_2, H_4, ...) seems a sensible choice of functions to fit to the data. We tried functions consisting of up to the 4th order Hermite polynomial. However the quality of the fit to only $\alpha H_0 + \beta H_2$ was equivalent to the sum of the first three even polynomials. Additionally, the inclusion of the 4th order term resulted in some high frequency oscillation in the deconvoluted data that seemed inappropriate. The resultant best linear least-squares fit to the data is shown as the solid line in Figure 6a and is a good representation of the data.

Gaussian instrumental functions with $\sigma = 0.08-0.1$ cm^{-1} were also generated (the 0.08 cm^{-1} function is the dotted line in the figure). The two smooth functions were transformed into Fourier space, divided out, and a subsequent Fourier transform resulted in the deconvolved Doppler profile of the HCO fragments shown as the dashed line in the figure. The deconvolution using an instrumental function with $\sigma = 0.10$ cm^{-1} was a little less flat at the center and slightly narrower, but otherwise quite similar to the profile shown.

The Doppler profile represents the distribution of v_x, the velocity in the direction of the laser propagation. The profile is also affected by the spatial anisotropy of the recoiling fragments (the $\mu-v$ vector correlation) and the presence of correlations between the rotation and velocity vectors (the $v-J$ correlation).[52,53] The propanal reaction is slow. It takes place via an intersystem crossing, and then after evolution on the triplet surface until the transition state is found. Any $\mu-v$ correlation (spatial anisotropy) must surely be washed out after this time.

We also assume no $v-J$ correlation and hence that the Doppler profile represents the true recoil velocity distribution. We use the v_x distribution in Figure 6a and integrate appropriately to obtain the speed distribution, and hence the translational energy distribution as shown in Figure 6b. We found that the final distribution is highly sensitive to (i) slight differences in the Hermite polynomial fit to the experimental profile and (ii) the width of the laser function used for the deconvolution. The shaded region in Figure 6b represents an indicative range of translational energy distributions from a variety of laser line widths and Hermite fitting functions. There is only a small effect on the low energy side of the distribution but a much more significant effect on the high energy side where the uncertainty in the distribution is quite broad. The reason for this is intuitively obvious—the high translational energy components of the fragments are represented in the extreme wings of the Doppler profile where there is very little intensity, and therefore, the most uncertainty. The distribution has been cut off at 15 kJ/mol because at the corresponding width in the Doppler profile the peak is just baseline noise. Nevertheless, the distribution clearly indicates that the most likely translational energy is ~6 kJ mol^{-1} and we calculate that the average translational energy is 6.5 ± 1.0 kJ mol^{-1}.

Discussion

Analysis of the experimental data above has provided a direct measurement of the threshold for photochemical production of CH_3CH_2 + HCO from propanal and hence an indirect measurement of the height of the barrier to reaction on the triplet surface. It has also yielded a wealth of information about the motion of nascent HCO following the reaction—a particularly detailed rotational distribution as a function of N, K_a, K_c, and J, and a translational energy distribution extracted from Doppler broadening in the spectrum.

In the discussion below we first investigate the overall thermochemistry of the reaction to fix, as best as possible, the available energy for the reaction products. Then we use the HCO energy distributions to infer information about the ethyl fragment using conservation of energy and linear momentum constraints. After establishing how the energy in both fragments is distributed we explore several models of a photodissociation reaction to elucidate the reaction mechanism. Finally, we examine closely the orientation of the HCO angular momentum in the body fixed frame (the K_a, K_c distribution) to provide information about the geometry of the HCO moiety at the transition state (t.s.).

(a) Thermochemistry of Reaction. One of our goals is to generate an energy level diagram of the important electronic states that play a role in the photodissociation of propanal (i.e., S_0, S_1, and T_1). The potential energy surfaces relevant to this study are shown in Figure 7. Following excitation of propanal from S_0 into S_1, the molecule can either fluoresce back to the S_0 state or undergo intersystem crossing onto the T_1 surface. The T_1 potential energy surface contains a barrier along the reaction coordinate of interest here (the C−C bond cleavage) leading to the formation of the radical products, CH_3CH_2 and HCO. The phofex spectrum shows that HCO products are not formed until 30 645 cm^{-1}, 581 cm^{-1} above the origin of the $S_1 \leftarrow S_0$ transition. Therefore, we conclude that the photochemical threshold for formation of HCO lies 366.6 kJ mol^{-1} above the zero-point of the S_0 state. This is slightly lower than that found in acetaldehyde (373.4 kJ mol^{-1},)[23] and we likewise associate this threshold with the top of the barrier to C−C bond cleavage on the T_1 surface.

The only remaining unknown salient quantities in Figure 7 are the T_1 zero-point energy level and D_0 the bond dissociation

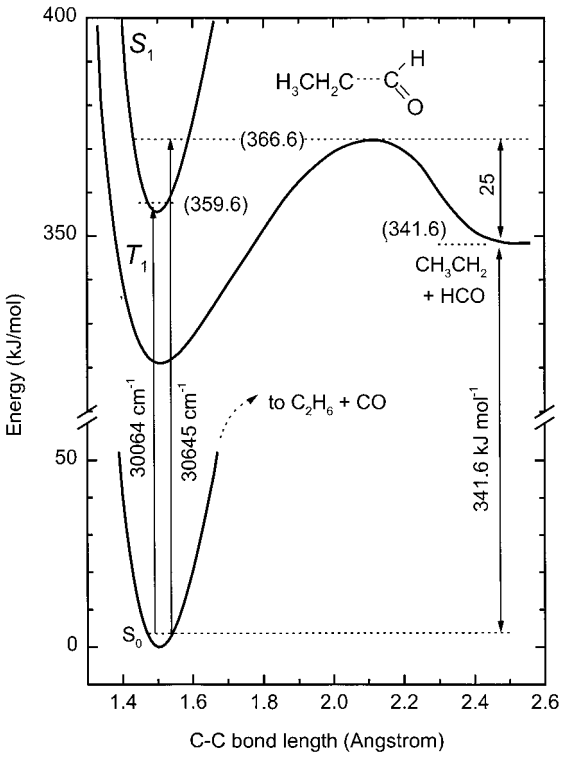

Figure 7. Potential energy curves for propanal along the reaction coordinate based upon spectroscopic and thermochemical information.

TABLE 1: Summary of Thermochemical Data Used in the Determination of ΔH_f, ΔH_r, and E_{avail}

species	298 K (kJ mol^{-1})	0 K (kJ mol^{-1})
ΔH_f (CH_3CH_2CHO)	−185.6 ± 0.9	−168.8± 0.9
ΔH_f (CH_3CH_2)	120.9 ± 1.9	131.4 ± 1.9
ΔH_f (HCO)	41.8 ± 0.8	41.4 ± 0.8
ΔH_r (CH_3CH_2CHO)	348.3 ± 3.6	341.6 ± 3.6
ΔE_{laser}		366.6
E_{avail} (CH_3CH_2 + HCO)		25.0 ± 3.6

energy, which when combined with any photon energy provides the energy available to be distributed into product motion, E_{avail}. This latter quantity can be estimated from the macroscopic thermochemical quantity, ΔH_r, which can be calculated from the experimentally known enthalpies of formation, ΔH_f, for propanal, CH_3CH_2, and HCO. Experimental enthalpies of formation at 298 K are well established for these molecules in the thermochemical literature and they can be related simply to the corresponding ΔH_f at 0 K by applying heat capacity corrections. Curtiss et al. have shown that this can be achieved easily and reliably by calculating these corrections from G2 ab initio theory.[54] We use the 298 K thermochemical values in Curtiss' paper for ethyl, formyl, and propanal, along with 0 K corrections for ethyl and formyl. New G2 calculations were performed on propanal to provide 0 K corrections for this molecule. We thereby calculate the overall enthalpy of reaction at 0 K to be 341.6 ± 3.6 kJ mol^{-1}. At threshold, the laser excitation energy is 366.6 kJ mol^{-1}. The difference, 25.0 ± 3.6 kJ mol^{-1}, is therefore E_{avail}, which in this case is also the height of the barrier for the reverse reaction on the T_1 surface. These results are summarized in Table 1.

(b) Energy Partitioning in the Fragments. Knowledge of the way the available energy, E_{avail}, is partitioned into the photofragment degrees of freedom can provide information on both energetics and dynamics of the reaction. The simplest means of achieving this is to calculate the *average* energy in each degree of freedom for each product. From the measurement

TABLE 2: Average Energy, $\langle E \rangle$, Deposited into HCO and CH_3CH_2 Fragments after Dissociation of Propanal near Threshold[a]

						impulsive models				
		experimental		statistical models			two-stick[b]			
molecule	degree of freedom	$\langle E \rangle$[b]	percent[c]	prior[c]	PST[c]	B&W[c]	$\gamma_2 = 0°$	$\gamma_2 = 90°$	$\gamma_2 = 40°$	γ_2=40°[d]
HCO	vibration	0	0%	4%	0%	29%	0%	0%	0%	0%
	rotation	2.5 ± 0.5	$10 \pm 2\%$	19%	29%		0%	28%	14%	11%
	translation	6.5 ± 1.5	$26 \pm 6\%$	9.5%	16%	21%	36%	26%	31%	26%
CH_3CH_2	internal	(9.5)	(38%)	58%	39%	29%	28%	20%	24%	36%
	translation	6.5 ± 1.5	$26 \pm 6\%$	9.5%	16%	21%	36%	26%	31%	26%
	total	25	100%	100%	100%	100%	100%	100%	100%	99%

[a] The first section is the experimentally determined values; the middle section is the results of statistical models; the right-hand section shows the calculated energy partitioning using different impulsive models. [b] kJ mol^{-1}. [c] percent of E_{avail}. [d] allowing 4 kJ mol^{-1} of vibrational energy in ethyl.

and analysis of the vibrational, rotational, and translational distributions we have a measure of the average rotational, vibrational, and translational energy, respectively, for HCO as summarized in Table 2. Since the ethyl and formyl fragments have the same mass, conservation of linear momentum dictates that the ethyl fragment must also possess $E_{trans} = 6.5$ kJ mol^{-1} on average. At threshold, the E_{avail} for the dissociation reaction is 25 kJ mol^{-1}, therefore, the remainder of the 9.5 kJ mol^{-1} of energy must be taken up in internal ethyl energy, distributed between vibration and rotation. These results are also summarized in Table 2.

(c) Existing Models of the Dissociation. *Statistical Models*. There is a large body of data to suggest that statistical theories of photodissociation perform well when the reaction occurs on a barrierless potential energy surface where the reaction is relatively slow and all degrees of freedom mix well through the exit channel. Statistical models assume that all microscopic product states are equally likely, given a series of constraints. The prior model conserves energy and linear momentum.[55] Phase space theory (PST) also includes conservation of angular momentum.[56,57] The constraints can be further limited by including the effects of a centrifugal barrier, or by limiting the size of the final impact parameter.

The reaction of propanal to form ethyl plus formyl is believed to take place over a barrier on the triplet surface. As such, statistical models should be inappropriate. Nonetheless, we calculated prior and phase space theory distributions in case the reaction dynamics measured here might suggest a different mechanism. Our calculations follow exactly those of previous authors.[44,56−58] Average energies for rotation, vibration, and translation of each fragment were calculated from these distributions and summarized in Table 2. Each statistical model predicts too little total translational energy (~19−32% versus >50% observed experimentally) and too much in internal energy, especially HCO, which has been measured explicitly here. Not only are the average energies seemingly inappropriate, but the energy distributions just seem to be qualitatively wrong, as shown by dashed curves in the lower panels of Figure 3 (rotational distribution) and Figure 6 (translational distribution). Therefore we confirm that the propanal reaction does not behave statistically, as expected, and we pursue impulsive models of photodissociation below.

Impulsive Models. Impulsive models are designed to explore the effect of the nuclear geometry on the resultant motion of the photofragments. One of the simplest and earliest models was devised by Busch and Wilson (BW) to model NO_2 dissociation.[59] The model has been used frequently since and undergone several modifications to accommodate specific reaction dynamics. First developed for atom−diatom systems, it was later extended to polyatom−polyatom half collisions.[60] The impulsive model assumes that upon excitation, all the photon energy is deposited straight into the reaction coordinate, in this case the C−C bond, and that a steep repulsive potential is present along this coordinate. The C−C bond is then assumed to break instantaneously to create two decoupled fragments and any subsequent energy flow between the fragments is not permitted. Each carbon atom shares the impulsive energy and each suffers an inelastic collision with the rest of the respective fragment, thereby transferring the repulsive potential energy into translation, rotation, and vibration of the two fragments. The model conserves the linear and angular momentum and energy.

The modified BW model can be compared with experiment without invoking any t.s. geometry. The predicted translational energy is independent of the t.s. geometry since it relies only on the masses of the atoms on either side of the breaking bond and the total mass of each fragment. Since a C−C bond is broken here, each carbon atom receives initially 50% of the impulsive energy. In the propanal reaction, both fragments have the same mass (29 amu) and the final translational energy is $(12/29) \times 50\% = 21\%$ of the available energy. The remaining energy is partitioned into internal energy of the formyl and ethyl fragments (29% each). The t.s. geometry only governs how this internal energy is partitioned into vibrational and rotational energy.

Comparison with the experimental data in Table 2 shows that the fraction partitioned into HCO internal energy (the most reliable experimental data) is three times higher in the model than the experiment. The BW model was derived initially for a directly repulsive potential energy surface, where the decoupling of the atom against the breaking bond from the rest of the fragment is most appropriate. The steepness of a repulsive surface allows coupling of the impulse into vibrational motion of the fragments. However, in the case where the impulse occurs after a t.s., the impulse will be much weaker (the slope of the surface is much shallower). This has been known for a long time, and represents the prototypical "late barrier" where the exit channel will couple energy primarily into rotation and translation of the fragments, but not vibration.

A modification of the impulsive model to cater for a "soft" impulse was considered by BW, and others, by considering the diatom bond to be infinitely stiff.[59,61,62] The vibrational energy in this case is considered to arise from vibrational motion at the t.s., distributed adiabatically into fragment vibration. The ideology of the model was used successfully by Moore and coworkers,[63] in explaining the photodissociation dynamics of ketene into CH_2 and CO. However, the problem with all these models, as far as our data are concerned, is that when the two atoms on either side of the breaking bond are the same, the total energy of each fragment is constrained to be half the available energy. This is a hangover from the original BW

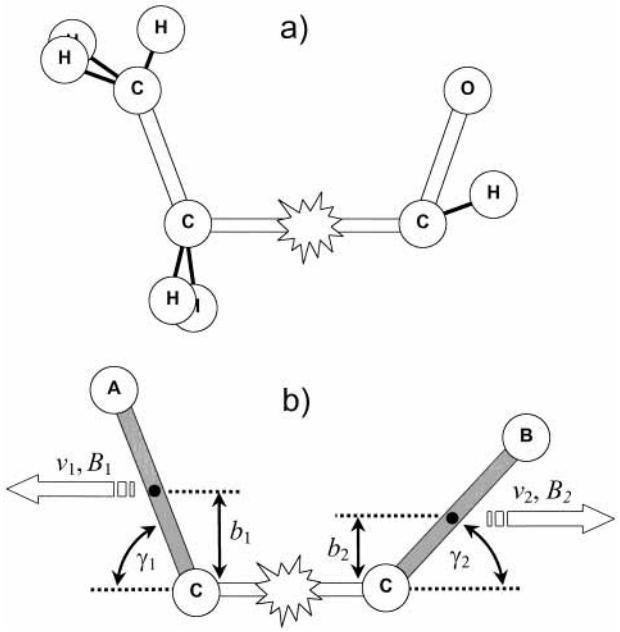

Figure 8. (a) A schematic representation of propanal dissociation and (b) the two-stick model where only the heavy atom framework is considered. Definitions of various properties are also indicated.

model, and in our case, seems not to be true—with the HCO fragment receiving about one-third of the available energy and the ethyl fragment two-thirds.

(d) The Two-Stick Model. We seek another simple impulsive model that contains all of the intuitive information of the previous models, but in which the fragment energies are not constrained artificially. The framework of propanal consists of four heavy atoms, dissociating to produce two pseudo-diatomic fragments. We use this heavy atom framework to develop a "two-stick" impulsive model.

Figure 8 shows the pseudo tetra-atomic system dissociating into two pseudo-diatomic fragments, CA and CB, along the C−C bond axis. The centers of mass of CH_3CH_2 and HCO were calculated from the structure of the isolated fragments and they are located at the correct place, at a distance r_i from the carbon atoms at each end of the breaking bond. Each stick has a mass of 29 amu and rotational constants, B, that are the same as the true polyatomic fragments. The rotational constants that we used were $\bar{B} = 1.447$ cm^{-1} from the known HCO rotational constants[64] and $\bar{B} = 0.77$ cm^{-1} from ab initio geometry of the ethyl radical.[65] Each fragment is initially aligned at some angle, γ_1 and γ_2, with respect to the C−C axis of the breaking bond. Associated with each fragment are two velocities, v_1 and v_2, two impact parameters, b_1 and b_2, and two rotational constants, B_1 and B_2. The system has a reduced mass, μ, and a relative velocity, $v = v_1 + v_2$.

We assume, in the same manner as previous impulsive models, that the bond breaks instantaneously, and that once broken there can be no exchange of energy between the departing fragments. The CA and CB bonds are sufficiently stiff in the sense that the impulse cannot couple energy into any vibrational motion. Vibrational motion of the fragments is assumed to arise solely from vibrational motion at the t.s. (none in the present case as the reaction occurs at threshold), and from relaxation of the nuclei from the t.s. nuclear configuration to the final product configuration. The probability of each vibrational coordinate being populated can then be evaluated via a Franck−Condon overlap. This separation of vibrational motion from rotational and translational motion is not new and features in previous "soft" impulsive models. At this point we do not consider the effect of vibrational motion at the t.s., even zero-point motion, on the rotation of the products.

The angular momentum, $J_i\hbar$ of each fragment, i, is calculated by considering the orbital angular momentum, $L_i\hbar$, of each fragment independently:

$$L_i\hbar = -J_i\hbar = \mu v \times b_i \tag{7}$$

where μ is the reduced mass of the HCO/CH_3CH_2 pair, v is the total relative velocity of the recoiling pair, and b_i is the impact parameter between the breaking bond and the center-of-mass of the fragment, i, as defined in Figure 8. The total orbital angular momentum for the recoiling fragments, $L\hbar = |\mathbf{L_1} + \mathbf{L_2}|\hbar$ can vary enormously for different orientations of the CA and CB fragments, even for the same γ_1 and γ_2, and therefore the same J_1 and J_2. For example in the cis geometry, as shown, $\mathbf{L_1}$ and $\mathbf{L_2}$ almost cancel, $L = L_1 - L_2$, and the fragments will be counter-rotating. In the trans geometry the orbital angular momentum adds and the fragments are conrotary.

The rotational energy of each fragment can be written as

$$E_i^{\mathrm{rot}} = B_i \times J_i(J_i + 1) \tag{8}$$

The total translational energy of the two fragments is simply

$$E_{1+2}^{\mathrm{trans}} = \frac{1}{2}\mu v^2 \tag{9}$$

which, in our case, is partitioned equally between the two fragments because they have the same mass. The rotational constants are 1.447 and 0.77 cm^{-1} for the formyl[64] and ethyl[65] radicals, respectively. Final closure of these equations arises from the conservation of energy requirement:

$$E_{\mathrm{avail}} = E_{1+2}^{\mathrm{trans}} + E_1^{\mathrm{rot}} + E_2^{\mathrm{rot}} \tag{10}$$

The t.s. structure affects the distribution of product energies through the impact parameters, $b_i = r_i \sin(\gamma_i)$. For any two angles, γ_1 and γ_2, there is only one solution for E_{1+2}^{trans}, E_1^{rot}, and E_2^{rot}.

We do not directly measure anything about the ethyl fragment and there have been no ab initio calculations of the t.s. structure. We therefore used parameters in the model by assuming the geometry is similar to the $CH_3CHO \rightarrow CH_3 + CHO$ reaction, which has been studied theoretically.[66] In that work, it was found that the methyl group becomes almost planar at the t.s. of the reaction surface with a CCH angle of ~100°. If we assume that the ethyl radical behaves like a methyl radical with a H-atom replaced by a CH_3 group, then the CCC angle between the C−C bond of ethyl and the leaving carbon atom of the formyl group would likewise be 100°. We have used this angle ($\gamma_1 = 80°$) throughout and not treated it as adjustable in any way.

The results from the two-stick model are shown in Table 2 for two limiting HCO angles: $\gamma_2 = 0°$ and 90° and no vibrational energy in ethyl. Not surprisingly, the amount of rotational energy in HCO is the quantity that varies most with this change. However, the model now allows energy to be partitioned unequally into HCO and CH_3CH_2. The HCO fragment may receive between 36% ($\gamma_2 = 0°$) and 54% ($\gamma_2 = 90°$) of the available energy. This occurs even though both the masses of the departing atoms (carbon) and departing fragments are the same and arises because if the bonds are infinitely stiff (compared to the impulse of the breaking bond) then the mass of the whole diatomic molecule comes into play. For example,

for $\gamma_2 = 0°$, the impulse of the breaking bond acts on the whole mass of the CB fragment, whereas for $\gamma_2 = 90°$, the impulse only acts on the adjoining carbon atom. If the CA (ethyl) angle was allowed to vary then the energy deposited into rotation and translation of each fragment could vary even further.

The observed experimental average energy distributions are best matched for an angle $\gamma_2 \approx 40°$, the results of which are also shown in Table 2. The model and experimental average energies are in quite good agreement at this angle, and the differences are within experimental error. Nonetheless, the HCO rotational and translational energy each seem a little high. Changing γ_2 can lower each of these, but only at the expense of raising the other. The reason may be that we have not allowed for any vibrational energy in the ethyl fragment (we have determined that there is no vibrational energy in HCO). We have discussed above that there has been no calculation of the propanal t.s. structure, but that based on the calculated t.s. structure of the acetaldehyde reaction, the methylene group in ethyl might be distorted by ~10° from planar. The ethyl radical is almost planar about the methylene group.[65] Therefore the ethyl moiety must relax from its pyramidal t.s. structure to its final, almost planar equilibrium structure. This relaxation will result in vibration along this normal coordinate. The frequency of the methylene umbrella vibration in ethyl is about 400 cm^{-1}. A distortion of 10° from planar into the t.s. structure requires about 4 kJ/mol and corresponds to 1 quantum of umbrella vibration.[65]

In the final column of Table 2 we have allowed ethyl to have 4 kJ mol^{-1} of vibrational energy and recalculated the translational and rotational distributions. The agreement between the model and the experimental average energies is quantitative, though the closeness of the agreement is probably fortuitous.

We can use the model above to investigate the range of angular momentum in HCO that might be expected from propanal dissociation at threshold. First, we examine the *largest* angular momentum that is possible within the model. The largest angular momentum occurs for $\gamma_2 = 90$. For the ethyl parameters discussed above (i.e., $\gamma_1 = 80°$) the maximum angular momentum corresponds to $J = 20$, or if ethyl is allowed to have 4 kJ mol^{-1} of vibrational energy, $J = 18$. The last observed peak in the HCO spectrum corresponded to $J = 19$ (see Figure 3) so not only the average rotational energy, but also the maximum angular momentum is in close accord with a simple impulsive model.

(e) Resolving Angular Momentum about the *b* and *c* Axes. In a near-prolate rotor, such as HCO, the degeneracy of rotation about an axis perpendicular to the symmetric top axis is broken. This is manifest in the spectrum of HCO as the asymmetry splitting for all transitions with $K_a > 0$. The splitting is largest for $K_a = 1$. Relative populations were measured for each of the rotational states with the same N, K_a as shown in Figure 5. As described above, there is a factor of 2−3 enhancement of the population in the state with slightly more energy, N_1^u over the lower energy partner, N_1^l.

The preference for HCO fragments to populate N_1^u has been seen previously in the dissociation of acetaldehyde.[23] This preference may be explained either classically or quantum mechanically. Figure 9 shows two limiting cases of propanal dissociation from the perspective of the HCO fragment; Figure 9a shows the recoiling R group leaving in the HCO plane, while Figure 9b shows the R group leaving out-of-plane. The torque exerted in case "a" results in angular momentum about the *c* axis of HCO, while case "b" results in a.m. about the *a/b* axes (predominantly the *b* axis). Classically, motion about the *c*-axis requires lower energy than motion about the *b*-axis and therefore

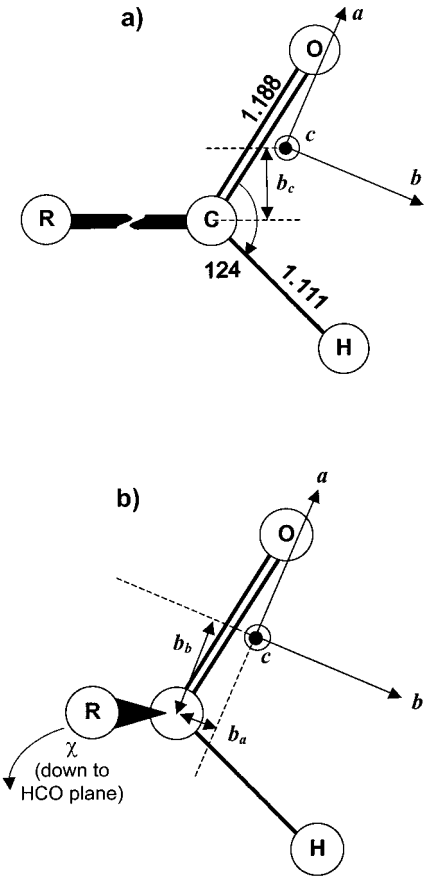

Figure 9. Two limiting cases for the HCO product with respect to the impulsive force acting on the carbon atom. (a**)** Impulse in the plane of HCO, which causes HCO to rotate about its *c* axis; b**)** impulse perpendicular to the HCO plane causing rotation mostly about the *b* axis.

the experimental observation of a preference for N_1^u corresponds to a preference for rotation about the *b*-axis, which arises from an impulse exerted on an out-of-plane HCO by the departing ethyl fragment.

The quantum mechanical derivation of the same result requires some fairly complex angular momentum quantum mechanics. The roots of the derivation can be found in the texts of Zare[67] and Schinke.[68] The derivation for this specific case is outlined in the paper of Chen,[23] and in more detail in the thesis of Waugh.[69] The final result is

$$\frac{P(N_1^u)}{P(N_1^l)} = \frac{|\int_0^{2\pi} \sin\chi\varphi_{ts}(\gamma,\chi)\,d\chi|^2}{|\int_0^{2\pi} \cos\chi\varphi_{ts}(\gamma,\chi)\,d\chi|^2} \qquad (11)$$

where P is the probability of populating state N_1^u or N_1^l, and $\varphi_{ts}(\gamma,\chi)$ is the vibrational wave function of the propanal t.s. with respect to the in-plane (γ) and out-of-plane (χ) angles of the HCO moiety. χ is defined as 0 for the C-atom of the ethyl fragment lying in the HCO plane (see Figure 9). The definition of γ is essentially the same as Figure 8, but it does not matter as its dependence cancels in the present discussion. If we consider the t.s. wave function to be a δ function in γ and χ (i.e., the HCO is frozen in place), then eq 1 becomes[23,69]

$$\frac{P(N_1^u)}{P(N_1^l)} = \frac{\sin^2\chi}{\cos^2\chi} \qquad (12)$$

The observed experimental ratio of $P(N_1^u)/P(N_1^l) \approx 3$ which indicates that the most probable out-of-plane angle χ is equal to 60°.

If the t.s. state wave function is considered to be a Gaussian function in both in-plane and out-of-plane angles, which is reasonable as the experiments were performed at threshold and therefore one would expect zero-point motion in all degrees of freedom except the reaction coordinate, then it turns out that the results only depends on χ_e, the equilibrium angle, and not the width of the Gaussian.[23,69] Therefore the result of eq 12 holds also for a more realistic wave function and yields a value $\chi_e = 60°$ to model the experimental data.

(**f) Comparison with Theory.** The dissociative state in this reaction is undoubtedly the lowest lying triplet state. There is nothing known about the geometry of propanal in this state—at the equilibrium, nor at the transition state to breaking the C−C bond. There have been several computational papers concerning the geometry of acetaldehyde on its equivalent triplet surface, including one in which the transition state to HCO formation is identified.[66] In acetaldehyde, the t.s. was calculated to have a C−C═O angle of 104°, corresponding to $\gamma = 76°$ in the two-stick impulsive model. The HCO out-of-plane angle was calculated to be 77°. Both ab initio angles are more acute than the angles evaluated from modeling the experimental data ($\gamma = 40°$ and $\chi = 60°$). Several things might account for the discrepancy. First, the two-stick model relies implicitly on the angle of the ethyl fragment (for which nothing is known). Second, the impulsive model correctly accounts for angular momentum at infinite separation of the fragments. The t.s. is obviously at close separation (some 2.1 Å in acetaldehyde[66]). The two angles would only coincide if there was no exit channel interaction or anisotropy. It might be that in propanal the rotation of the HCO is slowed (both in-plane and out-of-plane) while traversing the exit channel. Finally, more trivially and more obviously, the ab initio calculations are for a different molecule and while it is tempting to consider the mechanism of dissociation between acetaldehyde and propanal to be similar, it is only an assumption used here for comparative purposes. At least one other closely related aldehyde, propenal, shows quite different HCO rotational motion, which is indicative of a different reaction mechanism.[50]

Conclusions

In this work we have established the threshold for propanal dissociating into ethyl and formyl fragments. The threshold lies at $E = 30645\ cm^{-1}$ (366.6 kJ mol^{-1}) and corresponds to a barrier on the triplet surface of 25 kJ mol^{-1} from the products side. The nascent energy disposal in all degrees of freedom of the HCO fragment was measured. On average, 26% of the available energy was deposited in translational motion of HCO and therefore also CH_3CH_2, while 10% was deposited in HCO rotation and none in vibrational motion. This leaves 38% that must be contained in ethyl internal modes. The reaction dynamics are dominated by the structure of the molecule at the transition state. A modified impulsive model successfully reproduced the experimental data provided that the HCO moiety was highly kinked out-of-plane. This out-of-plane structure results in more rotation about the *b*-axis than the *c*-axis. There might be some interaction in the exit channel which results in a slowing of the HCO rotation.

Acknowledgment. We appreciate the assistance of George Bacskay in performing the G2 ab initio calculations for the heat capacity correction factors in propanal and Siobhan Waugh, George McBane, and Meredith Jordan for helping to elucidate the quantum mechanical effect of K_c in the reaction. We gratefully acknowledge the financial support of the Australian Research Council for providing funds in support of this project and the Joint Laser Facility for providing one of the lasers used in this work.

References and Notes

(1) Lee, E. K. C.; Lewis, R. S. *Adv. Photochem.* **1980**, *12*, 1.
(2) Avouris, P.; Gelbart, W. M.; El-Sayed, M. A. *Chem. Rev.* **1977**, *77*, 793.
(3) Kato, H.; Baba, M. *Chem. Rev.* **1995**, *95*, 2311.
(4) Moore, C. B.; Weisshaar, J. C. *Annu. Rev. Phys. Chem.* **1983**, *34*, 525.
(5) Hansen, D. A.; Lee, E. K. C. *J. Chem. Phys.* **1975**, *63*, 3272.
(6) Campbell, I. M. *Energy and the Atmosphere: A Physical and Chemical Approach*, 2nd ed.; Wiley: New York, 1986.
(7) Findlayson-Pitts, B. J.; Pitts, J. N., Jr. *Atmospheric Chemistry: Fundamentals and Experimental Techniques*; Wiley: New York, 1986.
(8) Rogers, J. D. *J. Phys. Chem.* **1990**, *94*, 4011.
(9) Martinez, R. D.; Buitrago, A. A.; Howell, N. W.; Hearn, C. H.; Joens, J. A. *Atmos. Environ.* **1992**, *26A*, 785.
(10) Moule, D. C.; Walsh, A. D. *Chem. Rev.* **1975**, *75*, 67.
(11) Chandler, W. D.; Goodman, L. *J. Mol. Spectrosc.* **1971**, *37*, 33.
(12) Godunov, I. A.; Yakovlev, N. N.; Belozerskii, I. S. *Russ. J. Phys. Chem.* **1994**, *68*, 954.
(13) Peterson, M. R.; De Mare, G. R.; Csizmadia, I. G.; Strausz, O. P. *J. Mol. Struct.* **1981**, *86*, 131.
(14) Ohta, N.; Baba, H. *J. Phys. Chem.* **1986**, *90*, 2654.
(15) Noble, M.; Lee, E. K. C. *J. Chem. Phys.* **1984**, *80*, 134.
(16) Baba, M.; Nagashima, U.; Hanazaki, I. *J. Chem. Phys.* **1985**, *83*, 3514.
(17) Leighton, P. A.; Blacet, F. E. *J. Am. Chem. Soc.* **1933**, *55*, 1766.
(18) Parmenter, C. S.; Noyes, W. A., Jr. *J. Am. Chem. Soc.* **1963**, *85*, 416.
(19) Horowitz, A.; Calvert, J. G. *J. Phys. Chem.* **1982**, *86*, 3105.
(20) Gejo, T.; Takayanagi, M.; Kono, T.; Hanazaki, I. *Chem. Phys. Lett.* **1994**, *218*, 343.
(21) Kono, T.; Takayanagi, M.; Nishiya, T.; Hanazaki, I. *Chem. Phys. Lett.* **1993**, *201*, 166.
(22) Kono, T.; Takayanagi, M.; Hanazaki, I. *J. Phys. Chem.* **1993**, *97*, 12793.
(23) Lee, S.-H.; Chen, I.-C. *J. Chem. Phys.* **1996**, *105*, 4597.
(24) Terentis, A. C.; Stone, M.; Kable, S. H. *J. Phys. Chem.* **1994**, *98*, 10802.
(25) Allinger, N. L.; Hickey, M. J. *J. Mol. Struct.* **1973**, *17*, 233.
(26) Gupta, V. P. *Can. J. Chem.* **1985**, *63*, 984.
(27) Bell, S. *J. Mol. Struct.* **1994**, *320*, 125.
(28) Allinger, N. L.; Schafer, L.; Siam, K.; Klimkowski, V. J.; Van Alsenoy, C. *J. Comput. Chem.* **1985**, *6*, 331.
(29) Van Nuffel, P.; van den Enden, L.; van Alsenoy, C.; Geise, H. J. *J. Mol. Struct.* **1984**, *116*, 99.
(30) Metha, G. F.; Buntine, M. A.; McGilvery, D. C.; Morrison, R. J. S. *J. Mol. Spectrosc.* **1994**, *165*, 32.
(31) Durig, J. R.; Guirgis, G. A.; Bell, S.; Brewer, W. E. *J. Chem. Phys. A* **1997**, *101*, 9240.
(32) Klimkowski, V. J.; Van Nuffel, P.; van den Enden, L.; van Alsenoy, C.; Geise, H. J.; Scarsdale, J. N.; Schafer, L. *J. Comput. Chem.* **1984**, *5*, 122.
(33) Alekseev, V. N.; Godunov, I. A. *Russ. J. Phys. Chem.* **1993**, *67*, 89; *ibid.*, 448.
(34) Cheatham, C. M.; Huang, M.; Kelly, M. B.; Meinander, N.; Laane, J. 13th Austin Symposium on Molecular Structure, Austin, 1990.
(35) Godunov, I. A.; Yakovlev, N. N. *Russ. J. Phys. Chem.* **1993**, *67*, 318.
(36) Shand, N. C.; Ning, C.-L.; Pfab, J. *Chem. Phys. Lett.* **1997**, *274*, 354.
(37) Shand, N. C.; Ning, C.-L.; Siggel, M. R. F.; Walker, I. C.; Pfab, J. *J. Chem. Soc., Faraday Trans.* **1997**, 93, 2883.
(38) Blacet, F. E.; Pitts, J. N., Jr. *J. Am. Chem. Soc.* **1952**, *74*, 3382.
(39) Shepson, P. B.; Heicklen, J. *J. Photochem.* **1982**, *18*, 169.
(40) Shepson, P. B.; Heicklen, J. *J. Photochem.* **1982**, *19*, 215.
(41) Terentis, A. C.; Knepp, P. T.; Kable, S. H. *J. Phys. Chem.* **1995**, *99*, 12704.
(42) Terentis, A. C.; Knepp, P. T.; Kable, S. H. In *Laser Techniques for State-Selected and State-to-State Chemistry III*; Hepburn, J. W., Ed.; *Proc. SPIE* **1995**, *2548*, 328.
(43) Terentis, A. C.; Kable, S. H. *Chem. Phys. Lett.* **1996**, *258*, 626.
(44) Terentis, A. C.; Waugh, S. E.; Metha, G. F.; Kable, S. H. *J. Chem. Phys.*, **1998**, *108*, 3187.

(45) Waugh, S. E.; Terentis, A. C.; Metha, G. F.; Kable, S. H. In *Laser Techniques for State-Selected and State-to-State Chemistry IV*; Hepburn, J. W., Ed.; *Proc. SPIE* **1998**, *3271*, 36.
(46) Shiu, Y. J.; Chen, I.-C. *J. Mol. Spectrosc.* **1994**, *165*, 457.
(47) Lee, S.-H.; Chen, I.-C. *J. Chem. Phys*. **1995**, *103*, 104.
(48) Lee, S.-H.; Chen, I.-C.; Adamson, G. W.; Field, R. W. *J. Mol. Spectrosc.* **1996**, *182*, 385.
(49) Lee, S.-H.; Chen, I.-C. *J. Chem. Phys.* **1996**, *105*, 2583.
(50) Jen, S.-H.; Chen, I.-C. *J. Chem. Phys.* **1999**, *111*, 8448.
(51) Hougen, J. T.; Watson, J. K. G. *Can. J. Phys*. **1965**, *43*, 298.
(52) Houston, P. L. *Acc. Chem. Res.* **1989**, *22*, 309.
(53) Dixon, R. N. *J. Chem. Phys.* **1986**, *85*, 1866.
(54) Curtis, L. A.; Raghavachari, K.; Redfern, P. C.; Pople, J. A. *J. Chem. Phys.* **1997**, *106*, 1063.
(55) Levine, R. D.; Bernstein, R. B. *Acc. Chem. Res.* **1974**, *7*, 393.
(56) Pechukas, P.; Light J. C. *J. Chem. Phys.* **1965**, *42*, 3281.
(57) Pechukas, P.; Light, J. C.; Rankin, C. *J. Chem. Phys.* **1966**, *44*, 794.
(58) Hunter, M.; Reid, S. A.; Robie, D. C.; Reisler, H. *J. Chem. Phys.* **1993**, *99*, 1093.
(59) Busch, G. E.; Wilson, K. R. *J. Chem. Phys.* **1972**, *56*, 3626.
(60) Trentelman, K. A.; Kable, S. H.; Moss, D. B.; Houston, P. L. *J. Chem. Phys.* **1989**, *91*, 7498.
(61) Tuck, A. F. *J. Chem. Soc., Faraday Trans. 2* **1977**, *73*, 689.
(62) Levine, H. B.; Valentini, J. J. *J. Chem. Phys.* **1987**, *87*, 2594.
(63) Chen, I.-C.; Moore, C. B. *J. Phys. Chem.* **1990**, *94*, 269.
(64) Brown, J. M.; Radford, H. E.; Sears, T. J. *J. Mol. Spectrosc*. **1991**, *148*, 20.
(65) Suter, H. U.; Ha, T.-K. *Chem. Phys.* **1991**, *154*, 227.
(66) Yadav, J. S.; Goddard, J. D. *J. Chem. Phys.* **1986**, *84*, 2682.
(67) Zare, R. N. *Angular Momentum. Understanding Spatial Aspects in Chemistry and Physics*; Wiley: New York, 1988.
(68) Schinke, R. *Photodissociation Dynamics*; Cambridge University Press: Cambridge, 1995.
(69) Waugh, S. E. Ph.D. Thesis, University of Sydney, 2002.